AREVA

Pipe Rupture External Loading Effects on U.S. EPR™ Essential Structures, Systems, and Components

ANP-10318NP
Revision 2

Technical Report

December 2013

AREVA NP Inc.

(c) 2013 AREVA NP Inc.

Copyright © 2013

AREVA NP Inc.
All Rights Reserved

Nature of Changes

Revision	Section(s) or Page(s)	Description and Justification
000	All	Original Issue
001	All	Body of report updated to include revised methodology for blast analysis
	Appendix A	Added CFD program and blast methods validation
	Appendix B	Added CFD blast sample problem analysis
002	3.3.2	Provided reference to Appendices A and B for development of analysis methodology
	3.4.1	Updated 3rd and 4th bullet
	3.4.1.3.1	Updated 1st bullet
	3.4.1.3.2	Clarified the blast loading method used for analysis
	Appendix B	Updated Figure references
	All	Editorial changes

Contents

Page

1.0 INTRODUCTION 1-1
2.0 CONCLUSIONS 2-1
3.0 PIPE RUPTURE EXTERNAL LOADING EFFECTS 3-1
3.1 Break Locations and Types 3-1
3.2 Jet Impingement 3-2
3.2.1 Source Conditions 3-3
3.2.2 Plume Effective Length and Maximum Thrust Coefficient 3-3
3.2.3 Jet Impingement Partial Intersection 3-9
3.2.4 Compressible Jet Properties 3-13
3.2.5 Jet Dynamic Loading and Resonance 3-17
3.2.6 Jet Deflection 3-25
3.2.7 Protection of Target Essential SSC 3-30
3.3 Blast Effects 3-30
3.3.1 Blast Source Potential 3-31
3.3.2 Analysis Methodology 3-33
3.4 Structural Evaluation of Typical Target Essential SSC 3-43
3.4.1 Dynamic Finite Element Analysis 3-44
3.4.2 Static Analysis using Dynamic Load Factors 3-54
3.4.3 Analysis Methodology Steps 3-55
3.5 Applicable Codes and Standards 3-57
3.5.1 Pressure Vessel Code Requirements 3-57
3.5.2 Steel Structure Code Requirements 3-58
3.5.3 Concrete Structure Code Requirements 3-58
4.0 REFERENCES 4-1
APPENDIX A CFD CODE VALIDATION A-1
APPENDIX B CFD SAMPLE PROBLEM B-1

List of Tables

Table 3-1: Thrust Coefficient (C_T) 3-9
Table 3-2: Exit Plane and Jet Conditions 3-16
Table 3-3: Jet Minimum Resonance Frequencies 3-20
Table 3-4: CFD Analysis Base Settings 3-35
Table 3-5: Steam Pipe Rupture Validation Parameters 3-36
Table A.3-1: Summary of Reference Settings for Blast Wave Application A-8
Table A.4-1: Reference 2D Mesh for the First Configuration A-17
Table A.4-2: Used 2D Meshes for the Second Configuration A-19
Table A.4-3: Overpressure Peak Obtained as Function of the Input Data for Incoming Blast Wave A-31
Table B.2-1: CFD Model Mesh Development Data B-5
Table B.2-2: Validated CFD Analysis Base Settings B-7

List of Figures

Figure 3-1: Partial Intersection 3-11
Figure 3-2: Partial Intersection 3-12
Figure 3-3: Partial Intersection 3-12
Figure 3-4: Strouhal Number for Subsonic Axisymmetric Modes 3-21
Figure 3-5: Strouhal Number for Supersonic Helical Modes 3-21
Figure 3-6: Dynamic Load Factor – Sinusoidally Varying Load 3-24
Figure 3-7: Jet Deflection Schematic 3-27
Figure 3-8: Jet Deflection Methodology 3-29
Figure 3-9: Typical Blast Wave Pressure-Time Curve 3-31
Figure 3-10: Model of a Pipe Containing a High-Energy Fluid and a Longitudinal Rupture Area 3-34
Figure 3-11: Model of a Steam Pipe Rupture in a Room 3-36
Figure 3-12: Pressure Time History for Test Case 3-39
Figure 3-13: Test Case Corner Pressure Time History 3-40
Figure 3-14: Test Case Pressure Time History at the Wall 3-41
Figure 3-15: Rectangular Plate Mode Shapes 3-52
Figure 3-16: Typical Plate and Shell Finite Element Model 3-53
Figure 3-17: Shell Stress Intensity vs. Load Frequency 3-54
Figure 3-18: Loading Analysis Methodology Flow Chart 3-56
Figure A.2-1: Simplified Blast Wave Formation from a High-Energy Line Rupture A-2
Figure A.2-2: Typical Blast Pressure-Time History A-2
Figure A.4-1: Experimental Test Configuration (Reference 29) A-10
Figure A.4-2: Dimensions of the Shock Tube Test and Positions of the Pressure Transducers A-11
Figure A.4-3: CFD 3D-Model and Boundary Conditions A-14
Figure A.4-4: Pressure-Time Profile Used as Input for Simulations (Red line) A-15
Figure A.4-5: Peak Pressure of a Blast Wave Propagation as Function of Distance (Reference 34) A-15
Figure A.4-6: Comparison of Experimental and Calculated Interferograms A-18
Figure A.4-7: Comparison of 2D and 3D Models Using the Coarse Mesh A-20
Figure A.4-8: Comparison between Turbulent and Inviscid Flow A-21

Figure A.4-9: Comparison between "Ideal Gas" and "Real Gas" A-22
Figure A.4-10: Comparison between Models Using Different Meshes A-24
Figure A.4-11: Comparison between Models Using Different Mesh Sizes A-25
Figure A.4-12: Comparison between Models using Different Courant Numbers A-26
Figure A.4-13: Comparison between Models Using Different Parameters D_{outlet} A-27
Figure A.4-14: Pressure-Time History in Position 1 from Experiments and from Simulations using Two Different Parameters D_{inlet} A-29
Figure A.4-15: Deviation in the Pressure-Time History Caused by the Reflected Wave from the Inlet Boundary A-30
Figure A.4-16: Comparison between Measured and Calculated Pressure-Time History A-34
Figure A.4-17: Comparison between Measured and Calculated Pressure-Time History at Position 3 ..... A-34
Figure A.4-18: Comparison between Measured and Calculated Pressure-Time History at Position 4 ..... A-35
Figure A.4-19: Experimental Configuration of the Detonation of Propane in Front of a Parallelepipedic Structure A-36
Figure A.4-20: CFD Model (Left) and Mesh (Right) of the Experiment A-38
Figure A.4-21: Measured and Calculated Reflected Pressure-Time Histories A-40
Figure B.2-1: Sample Problem Geometry – Plan View B-2
Figure B.2-2: Sample Problem Geometry – Elevation View B-3
Figure B.2-3: CFD Model Internal Structures and Initial Conditions B-4
Figure B.2-4: Elevation View of N4 and N5 Meshes at Plane through Pipe Rupture Point B-6
Figure B.2-5: Plan View of N4 and N5 Meshes at Plane through Pipe Rupture Point B-6
Figure B.3-1: Monitor Points in the Jet Stream Path B-9
Figure B.3-2: Wall Monitor Points B-10
Figure B.4-1: Blast Wave Characteristics at Time = 0.000392 sec B-16
Figure B.4-2: Elevation View of Pressure Field vs. Time B-17
Figure B.4-3: Plan View of Pressure Field vs. Time B-18
Figure B.4-4: Pressure Time History Curve for Monitor Points B-19
Figure B.4-5: Blast Pressures vs. Time B-19
Figure B.4-6: Steam Impingement on Walls at Time = 0.00866 Seconds B-20

Figure B.4-7: Steam Plume and Distribution at Time = 0.00403 Seconds B-20
Figure B.4-8: Target Wall Pressure Time Histories B-21
Figure B.4-9: Target Wall Corner Region Pressure Time Histories B-22
Figure B.4-10: Left Wall Pressure Time Histories B-22
Figure B.5-1: Mesh Specific Target Wall Pressure Time Histories (Points 1 – 8)..... B-25
Figure B.5-2: Mesh Specific Target Wall Pressure Time Histories (Points 9 – 16).... B-26
Figure B.5-3: Mesh-Specific Target Wall Pressure Time Histories (Points 17 - 18) B-27
Figure B.5-4: Meshes N5 and N6 Pressure Peak Deviations B-27
Figure B.5-5: Meshes N4 and N6 Pressure Peak Deviations B-28
Figure B.5-6: Meshes N1 and N6 Pressure Peak Deviations B-28

Nomenclature

(If applicable)

Acronym	Definition
ACI	American Concrete Institute
AISC	American Institute of Steel Construction
ASME	American Society of Mechanical Engineers
AUSM	Advection Upstream Splitting Method
BC	Boundary Condition
CFD	Computational Fluid Dynamics
DLF	Dynamic Load Factor
GGNB	Green Gauss Node Based Algorithm
HELBA	High Energy Line Break Accident
HEM	Homogeneous Equilibrium Model
MSL	Main Steam Line
NPR	Nozzle Pressure Ratio
NRBC	Non Reflecting Boundary Condition
NRC	Nuclear Regulatory Commission
PWR	Pressurized Water Reactor
RNG	Re-Normalization Group
SDOF	Single Degree of Freedom
SSC	Structures, Systems, and Components
UDF	User defined function

ABSTRACT

External loading effects on essential structures, systems, and components (SSC) of nuclear power plants are considered in accordance with the requirements of Reference 1. In the past, methods provided by Reference 2 have been used to determine the magnitude of the jet impingement loadings and the effects due to the unsteady nature of the fluid jet and the possible blast effects were ignored. As indicated in References 1, 3, and 4, the NRC has determined that some assumptions related to jet expansion modeling in the ANSI/ANS 58.2 standard may lead to nonconservative assessments of the jet impingement loads of postulated pipe breaks on neighboring SSCs. The NRC noted in Reference 1 that they are assessing the technical adequacy of the information pertaining to dynamic analyses models for jet thrust force and jet impingement load that are included in References 1 and 2. Pending completion of this effort, the NRC staff will review analyses of the jet impingement forces on a case by case basis. Therefore, analyses should show that jet impingement loadings on nearby safety-related SSCs will not impair or preclude their essential functions.

This report describes the AREVA NP methodology used to conservatively calculate the external loading effects on essential SSC due to jet impingement, including unsteadiness, and potential blast effects. In jet impingement loading, incompressible fluid jets, subcooled flashing jets, and single-phase steam jets are considered and the potential for resonance is evaluated. In blast loading, computer-based methods are provided to determine the loading on essential SSC, given the type and size of rupture and the location and configuration of nearby SSC.

The conservative nature of the methods discussed in this report provide a robust design and, per Reference 1, provide methods to demonstrate that external loading effects on nearby safety-related SSC will not impair or preclude their essential functions.

1.0 INTRODUCTION

This report describes the methods used to define the loading, to determine the response, and to perform structural evaluations for essential SSC because of the external effects of ruptures in high-energy fluid system piping in the U.S. EPR™. The external effects of piping ruptures discussed in this report include jet impingement and blast effects. Simplified approaches are used to define the loadings and are intended to bound the actual external loadings that would be experienced in the unlikely event of a guillotine rupture in a high-energy fluid system piping line.

The following areas are specifically investigated to define the loading, determine the response, and perform the structural evaluations; with appropriate methods being provided for their inclusion in the analysis effort:

1. Jet Impingement, considering:
    a. Plume Effective Length.
    b. Thrust Coefficient.
    c. Jet Resonance.
    d. Jet Deflections.
2. Blast Effects, considering:
    a. Energy Release.
    b. Target Distance.
    c. Overpressure and Impulse.
    d. Secondary Shock Effects.
3. Loading Analysis, considering:
    a. Dynamic Analyses using Finite Element Analysis.
    b. Static Analyses using Dynamic Load Factors.

4. Structural Evaluation, considering:

    a. ASME Code for Piping and Components.

    b. AISC for Steel Structures.

    c. ACI for Concrete Structures.

This report represents a departure from past pipe rupture effects design methods in two areas: (1) the jet impingement from subcooled flashing jets, and (2) single-phase steam jets and blast waves from ruptured steam lines. The methods provided in this report represent conservative approaches to define the loading constituents due to jet impingement using hand calculations and due to blast effects using Computational Fluid Dynamics analyses.

2.0 CONCLUSIONS

Based on the calculations and evaluations provided in this report, the following conclusions are obtained:

1. Break Locations and Types – Break locations and types are discussed in Section 3.1 and are determined in accordance with Reference 5.
2. Jet Impingement
   a. Source Conditions – Source conditions used to perform jet impingement calculations as they vary with time after the rupture, and their determination, are discussed in Section 3.2.1.
   b. Jet Plume Effective Length and Thrust Coefficient – [

      ]
   c. Compressible Jet Properties – Section 3.2.4 demonstrates that the exit plane conditions may be calculated using the [

      ]

d. Jet Resonance – As documented in Section 3.2.5, resonance in compressible jets can cause significant increases in the structural response of targets when the jet frequency is within 40% of the target structure frequency. [

]

e. Jet Deflections – As discussed in Section 3.2.6, jet deflections are possible for compressible and incompressible jets and should be considered in certain cases. A conservative method for consideration of jet deflection is to consider the secondary target as a primary target.

f. Protection of Target Essential SSC – As discussed in Section 3.2.7, essential SSC that cannot be demonstrated to meet code requirements under jet impingement loading must be protected by a jet shield. The jet shield is designed in accordance with applicable codes and standards to withstand the effects of jet impingement loading, resonant and non-resonant, and blast loading, as necessary.

3. Blast Effects – As discussed in Section 3.3, blast effects are evaluated using CFD software and can be important for SSC that lie within close proximity of the break. Blast effects may be amplified by the presence of walls, floors and ceilings. The overpressure and impulse forces that occur due to blast effects reduce quickly with respect to distance.

4. Structural Analysis – Methods used to perform loading analyses through the use of dynamic finite element analyses or static analyses are discussed in Section 3.4.

5. Code Compliance – Methods used to perform structural evaluations in accordance with applicable codes and standards are discussed in Section 3.5.

3.0 PIPE RUPTURE EXTERNAL LOADING EFFECTS

This section provides the basis for the determination of break locations and types, jet impingement loading and blast loading of target essential SSC.

3.1 *Break Locations and Types*

Piping failures are postulated to occur in high-energy fluid system piping in accordance with Reference 8. Per U.S. EPR FSAR Tier 2, Tables 3.9.3-1 and 3.9.3-2 pipe break loading (including jet impingement loading) on ASME Class 1, 2, and 3 components is considered a Service Level D event. Tables 3-1 and 3-2 of Reference 9 categorize high-energy line break and secondary-side pipe rupture loads as Level D events. As discussed in Reference 8, high-energy fluid system piping is defined as piping in which the normal operating conditions exceed 200°F or 275 psig. Failure locations in Class 1 and Class 2/3 piping are postulated in accordance with Reference 5, as follows:

- Class 1 Piping:
  - Terminal ends (circumferential breaks only).
  - Locations where the ASME Equations 10 and 12, or 10 and 13, stress ranges exceed 2.4 S_m (i.e., 80% of the ASME Code allowable).
  - Locations where the cumulative usage factor exceeds 0.1 (10% of the ASME Code allowable).
- Class 2/3 Piping
  - Terminal Ends (circumferential breaks only).
  - Locations where the sum of the ASME Equations 9 and 10 stress range exceeds $0.8(1.8S_h + S_A)$ (i.e., 80% of the ASME Code allowable).

Circumferential Break – These breaks are postulated at locations where the ratio of longitudinal stress to circumferential stress exceeds 1.5, in accordance with Reference 5.

Longitudinal Break – These breaks are postulated at locations where the ratio of longitudinal stress to circumferential stress is less than 1.5, in accordance with Reference 5.

Note that postulated longitudinal breaks are rare because the circumferential stress, caused by pressure, is maintained below approximately S_m in Class 1 piping. In order for a location to be considered a failure site in Class 1 piping, the stress must exceed 2.4 S_m, which indicates that the ratio of longitudinal stress to circumferential stress exceeds 2.4. This is greater than the maximum value of 1.5 that requires postulation of a longitudinal break. The ratio of longitudinal stress to circumferential stress in Class 2/3 piping is similar to that of Class 1 piping.

3.2 *Jet Impingement*

This section discusses source conditions, the plume effective length, the compressible jet velocity, jet resonance, and jet deflection. The source conditions for a jet typically change quickly after the rupture occurs, so a jet that begins as a non-flashing subcooled jet or a subcooled flashing jet may become a single-phase steam jet as the source pressure reduces. Jet impingement calculations must, therefore, be performed using varying source conditions for the full blowdown event; and consider the limiting conditions for the target SSC.

3.2.1 Source Conditions

Source conditions at the break are typically determined using a thermal-hydraulics code (e.g., RELAP or CRAFT2) that is capable of providing pressure and enthalpy as a function of time after the postulated rupture. Using the time-dependent source conditions of the blowdown event, from initial rupture through attainment of steady state, jet impingement calculations are performed to define the loading on target essential SSC. The following sections provide the methods used to define the loading.

3.2.2 Plume Effective Length and Maximum Thrust Coefficient

The behavior of a fluid jet from a ruptured pipe depends on the source conditions of the fluid in the pipe. Various reports and tests have been performed to characterize the jet plume geometries and to determine the distances at which the different types of jets can apply significant loading on targets. This section provides an evaluation to determine the appropriate effective lengths for use in U.S. EPR design.

This section also provides methods used to determine the maximum thrust coefficient for breaks with different source conditions. The thrust coefficient is defined as the exit plane thrust force divided by the product of source pressure and exit plane flow area. The exit plane thrust force for a given break represents the maximum jet impingement pulse force that can be delivered to a target SSC. In the case of two-phase source conditions, the maximum jet impingement force reduces with distance, as demonstrated in Reference 6 and discussed in Section 3.2.2.3.1. When considering oscillating jet impingement forces, the amplitude of the forcing function is conservatively considered equal to the jet impingement pulse force. This leads to a peak force equal to twice the jet impingement pulse force. Calculation of the thrust coefficient for incompressible liquid jets, steam jets, and subcooled flashing jets is discussed in detail in Sections 3.2.2.1.1, 3.2.2.2.1 and 3.2.2.3.1, respectively.

3.2.2.1 Incompressible Liquid Jets

Incompressible liquid jets occur when the source temperature is below the fluid boiling point under ambient conditions, typically 212°F. In this case, the velocity of the jet is significantly below the fluid's speed of sound; therefore, shock waves are not present. In this type of jet, there is no limit to the plume effective length, except that gravity will cause the jet to accelerate downward based on projectile motion calculations.

3.2.2.1.1 Incompressible Liquid Jet Maximum Thrust Coefficient

The jet thrust coefficient for an incompressible water jet may be calculated directly from Bernoulli's equation as follows:

Bernoulli's Equation (ignoring effects due to gravity):

$$P_0 + \rho_0 V_0^2 / 2 = P_1 + \rho_1 V_1^2 / 2$$

Where:

V_0 = Initial System Fluid Velocity

P_0 = Initial System Pressure

ρ_0 = Initial System Density

V_1 = Jet Fluid Velocity at Exit Plane

P_1 = Jet Pressure at Exit Plane

ρ_1 = Jet Fluid Density at Exit Plane

If P_0 is set to the system stagnation pressure, the dynamic pressure associated with fluid velocity prior to the rupture may be neglected. In addition, the exit plane pressure (P_1) approaches the ambient pressure for low temperature applications. This provides the following equation with appropriate reduction of terms:

$$P_0 = \rho_1 V_1^2 / 2 \Rightarrow 2P_0 = \rho_1 V_1^2$$

The impulse force at the exit plane of a fluid jet is calculated as follows, based on conservation of momentum principles:

$$F_1 = (P_1 + \rho_1 V_1^2) A_e \Rightarrow F_1 = \rho_1 V_1^2 A_e$$

Where:

A_e = Exit Plane Flow Area

F_1 = Exit Plane Impulse Force

Combining these two equations provides:

$$2P_0 A_e = \rho_1 V_1^2 A_e$$

The thrust coefficient is defined by the following formula:

$$C_T = F_1 / P_0 A_e = \rho_1 V_1^2 A_e / P_0 A_e = 2$$

Therefore, based on basic fluid mechanics principles, the maximum force of a jet at the pipe exit plane is defined as $2P_0A_e$, which indicates that the maximum jet thrust coefficient for an incompressible water jet is 2.0.

3.2.2.2 Single-Phase Steam Jets

Reference 10 documents test data used to determine the impact of jet impingement on various types of piping and component insulation used in nuclear power plants. Part of this test data focuses on single-phase steam jets. As discussed in that report (Reference 10, Section 1.1.3), single-phase steam jets with source pressures of 80 bars (≈1200 psia) can cause damage to insulation at a target distance of up to 25 times the pipe exit diameter (i.e., L/D = 25). The target essential SSC in a nuclear power plant, that are evaluated for loadings due to jet impingement, are of a construction that is significantly heavier than that of insulation. Therefore, these SSC would not experience similar damage from the relatively low jet momentum flux at this distance. Since some loading is to be expected, it is reasonable and conservative to assume that the jet is capable of applying full loading at this distance. [

]

3.2.2.2.1 Steam Jet Maximum Thrust Coefficient

From Reference 7 (Part 4.4), the dimensionless impulse function (Equation 4.23), which corresponds to the thrust coefficient, when considering the exit plane, as the control surface is as follows:

$$\frac{F}{P_0 A^*} = \frac{P}{P_0}\frac{A}{A^*}(1 + kM^2)$$

Where:

F = Exit Plane Force

P_0 = Stagnation Pressure

A^* = Throat Area = Exit Plane Area

P = Exit Plane Static Pressure

A = Exit Plane Area

k = Ratio of Specific Heats

M = Mach Number at Exit Plane

Considering that the throat is the location where $M = 1$, which is equivalent to the exit plane in this case, the term P/P_0 may be calculated from Eqn. 4.15b of Reference 7, as follows:

$$\frac{P^*}{P_0} = \frac{P}{P_0} = \left(\frac{2}{k+1}\right)^{\frac{k}{k-1}}$$

Where:

P^* = Throat Pressure = Exit Plane Static Pressure (P)

Combining these equations provides the following expression for thrust coefficient:

$$C_T = \left(\frac{2}{k+1}\right)^{\frac{k}{k-1}}(1+k)$$

The specific heat ratio for steam can vary with quality and pressure. However, for exit plane pressures between 14.7 psi and 750 psi and qualities between 1.0 and 0.9, the specific heat ratio lies between 1.3 and 1.7. Solving for C_T using this range of values provides a minimum of 1.26 and a maximum of 1.30.

3.2.2.3 Subcooled Flashing Jets (Two Phase Jets)

Reference 6 performs numerical analyses for subcooled flashing jets and compares the calculated data to various sources of test data. The report provides plots of target pressures and target forces versus distance from the break for two phase jets at various upstream initial conditions.

Section 3.2.2.3.1 provides a tabulation of the thrust coefficients found on the plots from Reference 6 for use in defining a simplified method of determining jet impingement forces.

3.2.2.3.1 Subcooled Flashing Jet Maximum Thrust Coefficient

Table 3-1 tabulates the thrust coefficient (C_T) as a function of pressure and target distance, as calculated from Figures A.1 – A.125 of Reference 6. As shown in the table, in most cases, the plots do not provide this information beyond L/D=10 because C_T is trending towards a negligible value prior to L/D = 10. The only case where C_T values are provided for L/D ratios greater than 10 is for a source pressure of 2200 psia and subcooling of 63°F. Even in this case, the maximum C_T value is 0.1 at an L/D = 12.5, which is considered negligible.

[

]

Table 3-1: Thrust Coefficient (C_T)

[ ]

Notes:

1. C_T is defined as the Target Force divided by P_0A_e and is taken as the maximum value for a given L/D and upstream pressure from the target load distributions plots from Figures A.1 – A.125 of Reference 6. The Max C_T is the maximum for any L/D for a given upstream pressure.
2. Plots of C_T at an L/D of 12.5 are not provided for any upstream pressures except for 2200 psia. In most cases, as shown in the table, the value of C_T reaches a negligible value prior to this distance. Also as shown in the table, although a value of C_T is plotted at L/D = 12.5 for a pressure of 2200 psia, the value of 0.1 may be considered negligible, particularly with respect to the conservatism in the "Max C_T" values plotted, which are significantly greater than the theoretical maximum of 2.0.

3.2.3 Jet Impingement Partial Intersection

[

]

[

]

Figure 3-1: Partial Intersection

[

]

Figure 3-2: Partial Intersection

Figure 3-3: Partial Intersection

3.2.4 Compressible Jet Properties

[ ] is used to determine the pipe rupture mass flow rate and exit plane conditions. [

] Note that the static pressure in the jet can reach values lower than the ambient pressure; however, this requires the jet to go through normal or oblique shocks to regain equilibrium with the atmosphere. The shocks result in conversion of kinetic energy to thermal energy and an increase in entropy. This process results in a loss of jet dynamic pressure and momentum flux. The following sections provide more detail on the analysis.

3.2.4.1 Exit Plane Conditions

The properties at the exit plane (e.g., pressure, enthalpy, velocity) are determined using the [

] The velocity may then be determined from the following equations:

$$h_0 = h_1 + V_1^2 / 2$$

Where:

h_0 = Enthalpy at Upstream Conditions

h_1 = Enthalpy at Assumed Exit Plane Conditions

V_1 = Velocity at Exit Plane Conditions

Rearranging provides:

$$V_1 = \sqrt{2(h_o - h_1)}$$

The exit plane mass flux is then calculated as follows:

$$G_1 = \rho_1 V_1$$

Where:

G_1 = Mass Flux at Exit Plane

ρ_1 = Density at Assumed Exit Plane Conditions

V_1 = Velocity at Assumed Exit Plane Conditions

3.2.4.2 Compressible Jet Velocity

[

]

$$h_0 = h_2 + V_2^2 / 2$$

Where:

h_0 = Stagnation Enthalpy at Upstream Conditions

h_2 = Enthalpy at Expanded Conditions

V_2 = Jet Velocity at Expanded Conditions

Since the flow is assumed to be isentropic, the downstream enthalpy can be calculated by determining the quality from the following relation:

$$x_2 = \frac{s_0 - s_f}{s_g - s_f}$$

Where:

x_2 = Quality at Fully Expanded Conditions

s_0 = Entropy at Initial Conditions (BTU/lbm-R)

s_f = Saturated Water Entropy at Atmospheric Pressure = 0.312 BTU/lbm-R

s_g = Saturated Steam Entropy at Atmospheric Pressure = 1.757 BTU/lbm-R

Assuming that the static pressure at expanded conditions is equal to the atmospheric pressure, the enthalpy at expanded conditions can be calculated. From this, the velocity can be determined, as follows:

$$V_2 = \sqrt{2(h_0 - h_2)}$$

Using this formulation, along with that of Section 3.2.4.1; the exit plane conditions, as well as the expanded jet conditions, are calculated in Table 3-2.

Table 3-2: Exit Plane and Jet Conditions

Initial Press. (P_0) (psia)	Initial Temp. (T_0)	Initial Enthalpy (h_0) (Btu/lbm)	Initial Entropy (s_0) (Btu/lbm-R)	Exit Plane Density (ρ_1) (lbm/ft^3)	Exit Plane Velocity (V_1) (ft/sec)	Jet Quality (x_2)	Jet Enthalpy (h_2) (Btu/lbm)	Jet Velocity (V_2) (ft/sec)
Two Phase Jets								
2250	650	695.20	0.88	20.2	448	0.395	563	2572
2250	565	566.02	0.76	45.0	478	0.311	482	2051
2250	350	325.13	0.50	55.7	590	0.129	306	992
2250	250	223.26	0.36	58.9	587	0.036	215	630
1500	575	581.36	0.78	42.9	231	0.324	494	2092
1500	565	567.90	0.77	43.3	269	0.314	485	2035
1500	350	323.93	0.50	55.7	473	0.130	307	933
1500	250	221.69	0.37	58.9	477	0.037	216	531
1000	540	536.63	0.74	26.6	212	0.294	466	1883
1000	500	487.73	0.69	49.0	248	0.260	432	1666
1000	350	323.13	0.50	55.7	376	0.131	307	892
1000	250	220.64	0.37	58.9	386	0.038	217	453
500	450	430.22	0.63	51.5	116	0.219	392	1378
500	350	322.35	0.50	55.6	241	0.132	308	848
500	250	219.60	0.37	58.8	266	0.038	217	358
250	375	348.34	0.54	54.7	92	0.154	330	961
250	250	219.08	0.37	58.8	177	0.038	217	299
Steam Jets (x_0=1.0)								
1250	572.5	1182	1.362	1.7	1468	0.727	885	3854
1000	544.7	1193	1.391	1.3	1499	0.747	905	3799
500	467.0	1205	1.464	0.7	1463	0.798	954	3547

3.2.4.3 Pulse Loading Definition

Pulse loading refers to the initial period of jet impingement loading which is characterized by a rapid rise time and a short period of relatively steady loading prior to the development of oscillating flow mechanisms. The ramp time for the initial pulse loading is considered as 1 millisecond, consistent with the guidance of Reference 1. The magnitude of the loading during this period is defined in Section 3.2.2 for each type of jet and is equal to the product of the thrust coefficient, the source pressure and the exit plane area, unless modified for consideration of partial intersections, as discussed in Section 3.2.3.

3.2.5 Jet Dynamic Loading and Resonance

In this section, the ability for jet resonance to adversely impact the loadings on essential SSC is evaluated. The calculation of minimum jet resonance frequencies for impinging jets, and the conditions in which resonance is unlikely, are based on the following papers:

1. References 11 and 12 provide test data and analysis used in determining the resonant frequencies of high speed subsonic jets ($0.7<M<1.0$) at target distances (L/D) less than 7.5 (Section 1 of Reference 12). Jets at these velocities with targets at these ranges are subject to traveling waves that cause localized variations in the pressure time histories applied to the target. These localized pressure-time histories can behave like a sine wave with narrow banded frequency content.
2. Reference 13 provides theoretical background and test data to determine the minimum resonant frequencies for axisymmetric and helical mode shapes for supersonic jets ($M>1.0$). It is also demonstrated that the results for subsonic jets match well with those of References 11 and 12. Therefore, the calculation of minimum resonance frequency is based on Reference 13.
3. Reference 14 provides an overview of many tests that have been performed on impinging jets. In this paper (Section IV.A) it is shown that, for cases in which the NPR exceeds 3.38 and the target distance (L/D) exceeds 5, there is no experimental

evidence indicating the existence of impingement tones. This is likely due to the existence of a strong normal shock near the nozzle exit in a converging nozzle. This indicates that resonance is unlikely in these cases.

4. [

]

3.2.5.1 Jet Resonance Minimum Frequency

Reference 13 provides the theory behind jet mode shapes and compares the theoretical data to experimental data. As demonstrated in Reference 13, the theoretical data and experimental data correlate very well. It is indicated that subsonic jets with Mach numbers between 0.7 and 1.0 are capable of supporting axisymmetric mode shapes while supersonic jets with Mach numbers greater than 1.0 are capable of supporting axisymmetric as well as helical mode shapes.

Based on review of the reference material discussed above (References 11, 12, 13, and 14), the following conclusions are drawn:

1. Supersonic and high speed subsonic (M>0.7) flows can generate significant pressure oscillations. The amplitude of the oscillations is discussed in Section 3.2.5.2.
2. Reference 14 demonstrates that tonal production is limited with NPR greater than 3.38 and L/D greater than 5. This indicates that resonance is unlikely in these conditions.

Reference 13 is used to determine the minimum frequencies for axisymmetric modes in supersonic jet flows. In that paper, the following equation (Equation 22), after rearrangement, is provided:

$$f = \frac{\sigma_i U_{jet}}{\pi D_{jet} M_{jet} (a_{jet} / a_\infty)(((a_\infty / a_{jet}) + M_{jet})^2 - 1)^{0.5}}$$

Where:

f = Minimum Axisymmetric Mode Resonance Frequency for Supersonic Jet

σ_i = First Positive Zero of the Order 1 Bessel Function ($J_1(x)$) = 3.83

U_{jet} = Jet Velocity

D_{jet} = Jet Diameter

M_{jet} = Jet Mach Number

a_{jet} = Jet Speed of Sound

a_∞ = Ambient Speed of Sound

As demonstrated in Reference 13, the frequencies of the subsonic axisymmetric modes and supersonic helical modes can be calculated using the Strouhal number for the jet. The Strouhal number is a dimensionless parameter that provides a measure of oscillating flow mechanisms and is calculated as follows:

$$St = \frac{fL}{V}$$

Where:

St = Strouhal Number

f = Frequency

L = Characteristic Length = Nozzle Diameter

V = Velocity

Reference 13 provides a plot of Strouhal number versus Mach number for axisymmetric modes in subsonic jets, which is provided herein as Figure 3-4. Reference 13 also provides a plot of Strouhal number versus Mach number for helical modes in supersonic jets, which is provided as Figure 3-5. The Strouhal number for the jet is taken from these plots based on the Mach number of the expanded jet conditions, calculated as explained in Section 3.2.2. Based on this information, the minimum resonance frequency can be determined for a given set of fluid conditions.

These frequencies are only the minimum frequencies for jet resonance. Resonance may also occur at higher frequencies, which must be considered in the structural analysis of the SSC. In cases where the target SSC has natural frequencies that are higher than the minimum frequency of the resonant jet, each of these higher frequencies is considered to coincide with a jet resonance frequency. In most cases, since the response of the SSC to higher frequency loading is limited, the response of the SSC at each frequency is reviewed to determine the limiting condition. Table 3-3 provides a tabulation of frequencies and speed of sound for various conditions and nozzle sizes calculated using the formula in Section 3.2.5.1, Figure 3-4, and Figure 3-5.

Table 3-3: Jet Minimum Resonance Frequencies

Pipe Diameter (in)	Jet Sound Speed (ft/sec)	Subsonic Jet Freq (M=0.7) (Hz)	Subsonic Jet Freq (M=0.9) (Hz)	Supersonic Jet Axisym. Freq (M=2) (Hz)	Supersonic Jet Helical Freq (M=2) (Hz)
4	1500	2205	1620	1130	1286
6	1500	1470	1080	753	857
10	1500	882	648	452	514
14	1500	630	463	323	367
18	1500	490	360	251	286
24	1500	368	270	188	214

Figure 3-4: Strouhal Number for Subsonic Axisymmetric Modes

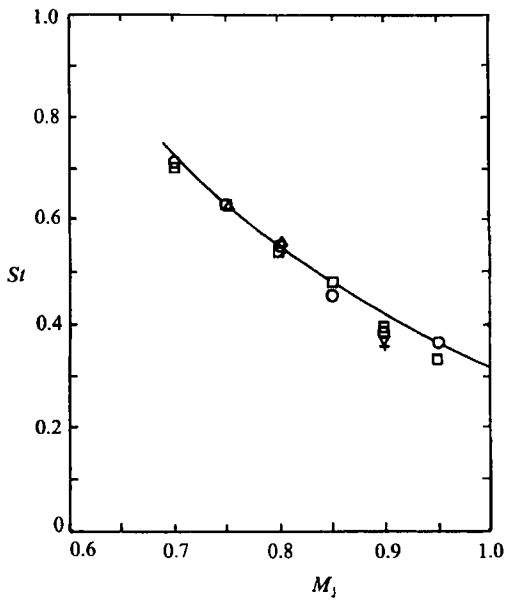

(Reference 13)

Figure 3-5: Strouhal Number for Supersonic Helical Modes

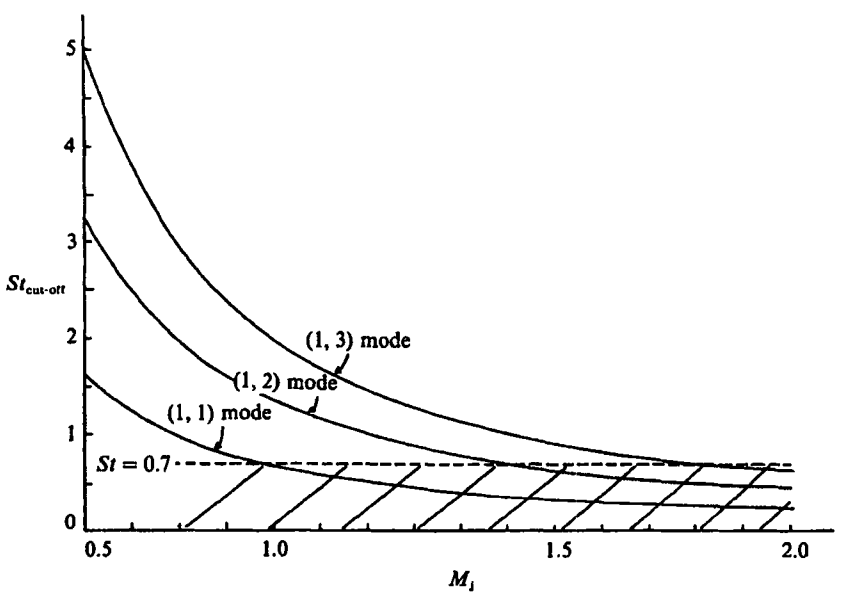

(Reference 13)

3.2.5.2 Jet Force Amplitude

Reference 15 provides a numerical analysis of supersonic impinging jet flow. As shown in Figures 7 and 12 of Reference 15, the amplitude of the pressure oscillation is shown to be as great as 45% of the stagnation pressure upstream of the exit plane.

Reference 16 provides a plot of the pressure time history at a location on the target as well as a plot of the target response time history, measured as forces in the target supports. As shown in Figure 7 of Reference 16, the measured pressure oscillates with an amplitude of approximately 13% of the average target pressure.

[

]

3.2.5.3 Total Response

[

]

3.2.5.3.1 Idealized Single Degree of Freedom Structures

Certain simple structures, such as pipe supports, whip restraints and jet shields, may be idealized as single degree of freedom (SDOF) structures. The response of these structures to static and dynamic loading may often be determined through hand calculations, using methods described in Reference 17, for example.

The initial pulse force provides a dynamic load factor of 2.0 for a target structure that can be considered as a SDOF structure, which leads to a maximum response load of $2C_T P_0 A_e$.

Based on Figure 3-6 from Reference 17, the Dynamic Load Factor (DLF) for an SDOF structure with a sinusoidal varying load and a damping value of less than 10% percent of critical, is less than 1.0 when the ratio of the frequency of the load (Ω) to the frequency of the structure (ω) is greater than 1.4. In other words, if the forcing function frequency is 40% greater than the target structure frequency, the DLF is a maximum of 1.0. As stated above, the range of the sinusoidal load (i.e., 2 x the amplitude) is equal to twice the jet force. Therefore, in cases where the frequency of the resonant jet is at least 40% greater than the frequency of the target structure, the response of an SDOF structure to a resonant jet is no greater than the steady jet pulse response.

This indicates that resonant jets do not require evaluation in cases where the minimum jet frequency is at least 40% greater than the target structure frequency.

3.2.5.3.2 Multi-Degree of Freedom Structures

Many target structures, such as large pressure vessels, have multiple degrees of freedom and are not conducive to analysis through hand calculations. In those cases, computer analyses are performed using force time histories with the appropriate frequency and amplitude. Structural evaluation of target structures using computer analysis techniques is discussed in greater detail in Section 3.4.

Figure 3-6: Dynamic Load Factor – Sinusoidally Varying Load

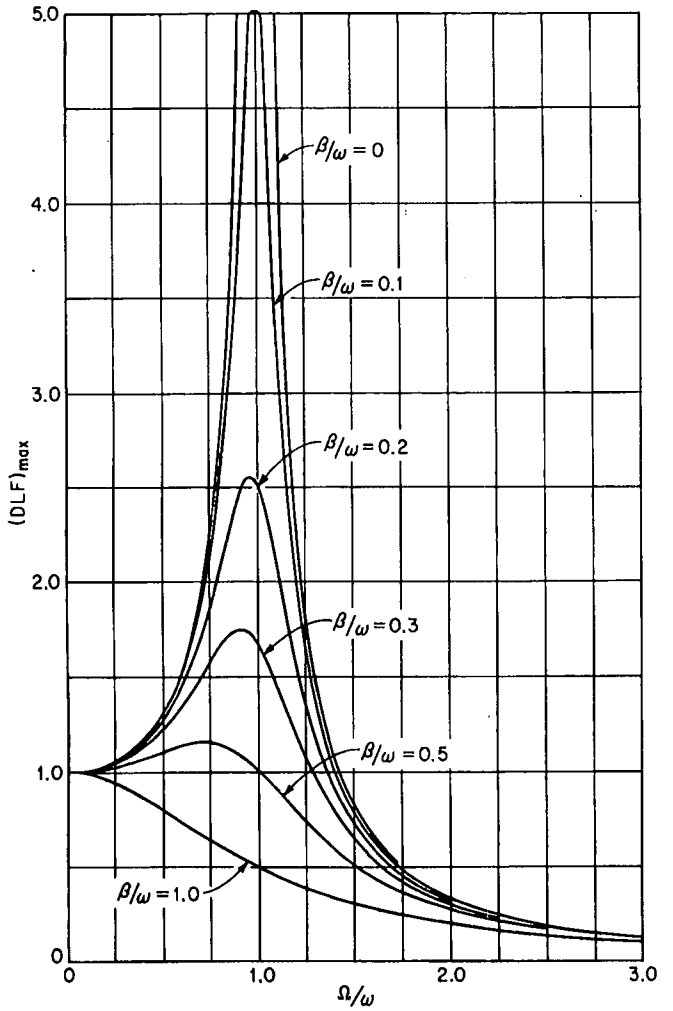

(Reference 17)

3.2.5.4 Random Unsteadiness

Unlike jet resonance, random unsteadiness in a fluid jet is a broadband phenomenon, much like turbulence. Because it is a broadband phenomenon, the amplitude of the forcing function at a given frequency is limited. Therefore, stresses in robust SSC (e.g., pressure vessels) are not a concern under these loadings.

Figure 3 from Reference 12 provides a comparison of the surface pressure fluctuation signal power spectra for a resonant (i.e., narrow-banded) jet at a Mach number of 0.8 and a non-resonant (i.e., broad-banded) jet at a Mach number of 0.5. The figure is comparing normalized power spectra, which indicates that the total area under each curve is equivalent. As shown in the figure, the maximum power in the resonant jet at its resonant Strouhal number (~0.5) is approximately 10 times the maximum power in the non-resonant jet. As power is proportional to the square of signal amplitude, this indicates that the amplitude of the pressure variations in the resonant jet are approximately 100 times the amplitude of the pressure variations in the non-resonant jet. The initial pulse loading from the jet is equivalent to that of a resonant jet; therefore, bounding the response from non-resonant jet loading. Based on this evaluation, consideration of broad-banded sources for loading of rugged structures is not required.

However, random unsteadiness can cause fatigue failures in lightly constructed SSC over time. Therefore, failure in lightly constructed SSC (e.g., valve operators, instrumentation) under jet impingement loading is assumed to occur unless protected by a jet shield, as discussed in Section 3.2.7.

3.2.6 Jet Deflection

Jet impingement loads on secondary targets due to jet deflection may occur in certain situations and are considered in this section. It is typically considered that a jet, whether it is incompressible or compressible, loses a significant amount of energy after striking the primary target. This section provides a method for consideration of the loading on a secondary target.

3.2.6.1 Jet Deflection – Incompressible Jet

Figure 3-7: Jet Deflection Schematic

3.2.6.2 Jet Deflection – Compressible Jet

The deflection of a supersonic compressible jet occurs through normal and oblique shocks that represent discontinuities in the flow stream. The two types of shocks and the associated loss of energy are discussed in the following subsections.

3.2.6.2.1 Normal Shock

In supersonic compressible jets, which are typical of most jets originating from high-energy piping systems, a normal shock exists upstream of the target SSC, as demonstrated by Reference 6. A normal shock is an irreversible process that causes the jet to lose kinetic energy and transforms the supersonic jet into a subsonic jet. The jet may then re-expand to become supersonic again; however, the momentum flux of the jet is reduced by the shock.

As shown in Reference 7, the entropy increases across the shock. When considered at equilibrium conditions, an increase in entropy corresponds to an increase in enthalpy. This indicates that some of the kinetic energy is transferred to thermal energy, reducing the velocity and density of the jet; therefore, the momentum flux is reduced.

The conclusion is that loading of a secondary target, one that is struck by the jet after passing through a shock and re-expanding to form a supersonic jet, is not as severe as loading of a primary target.

3.2.6.2.2 Oblique Shock

In the case of a supersonic compressible jet striking a target structure at a shallow deflection angle (i.e., large angle of incidence), the flow can change direction through an oblique shock and maintain supersonic velocity downstream of the shock. The maximum deflection angle that will allow downstream supersonic flow is dependent upon the jet's Mach number and specific heat ratio. As discussed in Reference 7 (Figures 16.4 – 16.6), flows with greater upstream Mach numbers can be deflected through greater angles, while maintaining supersonic conditions. For example, considering air with a specific heat ratio of 1.4, flow with a Mach number of 2.5 has a maximum possible deflection angle of 30° while flow with a Mach number of 1.5 has a maximum possible deflection angle of about 12°.

However, as demonstrated in Reference 7 (Part 16.3), oblique shocks, just like normal shocks, cause an increase in entropy. This has the effect of reducing the density and the velocity, which reduces the forces.

[

]

3.2.6.2.3 Secondary Target Loading

[

]

Figure 3-8: Jet Deflection Methodology

[

]

3.2.7 Protection of Target Essential SSC

Target essential SSC that cannot be demonstrated to be structurally acceptable in accordance with established codes and standards (such as ASME, ACI, and AISC) based on criteria of allowable stress or strain are considered "lightly constructed essential SSC" and must be protected to prevent failure. In most cases, active components powered by electricity or service air are considered to be components that cannot be qualified for jet impingement loading through analytical calculations. The protective structure may be designed as any type of structure, such as concrete or steel, that is capable of deflecting the jet and withstanding the external loading effects due to pipe rupture, including the effects due to resonance and random unsteadiness and blast effects, as necessary. Protective structures are considered safety-related structures and must meet the same code requirements as other target essential SSC, typically those of AISC (Reference 18) or ACI (Reference 19).

3.3 *Blast Effects*

[

]

[

]

Figure 3-9: Typical Blast Wave Pressure-Time Curve

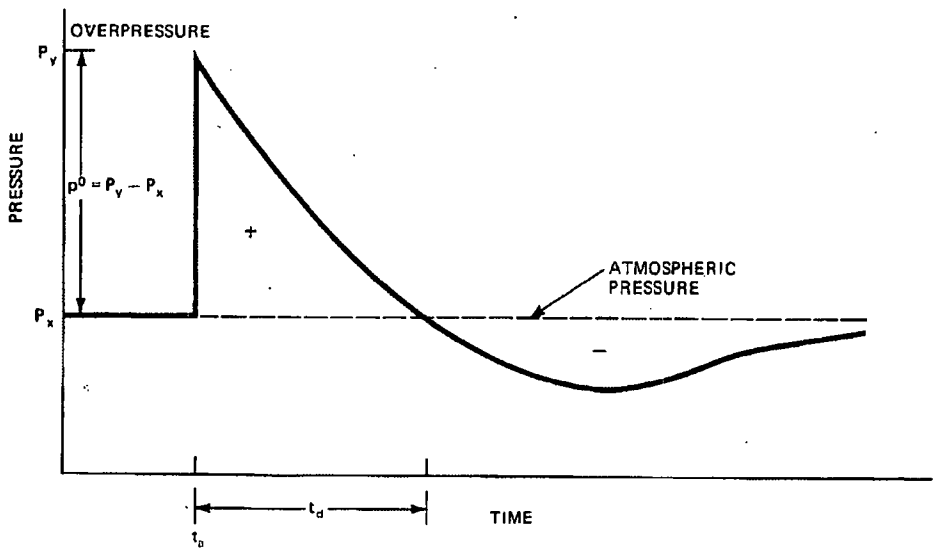

3.3.1 Blast Source Potential

[

]

3.3.1.1 Evaluation of Source Conditions

The following sections provide evaluations of the blast effects due to ruptures in subcooled water lines and steam lines.

3.3.1.1.1 Subcooled Water

[

]

3.3.1.1.2 Steam

[

]

[

]

3.3.2 Analysis Methodology

[

]

3.3.2.1 Energy Release

[

]

[

]

Figure 3-10: Model of a Pipe Containing a High-Energy Fluid and a Longitudinal Rupture Area

[ ]

The location of the break area in the pipe is selected to represent the worst scenario; i.e., as close as possible to a target essential SSC. The geometry of the room affects the possible pressure wave reflections and its amplification.

3.3.2.2 Basic Model Settings

[

]

Table 3-4: CFD Analysis Base Settings

3.3.2.3 Modeling Details

[

]

Table 3-5: Steam Pipe Rupture Validation Parameters

[ ]

Figure 3-11: Model of a Steam Pipe Rupture in a Room

[ ]

[

]

[

]

Figure 3-12: Pressure Time History for Test Case

[

]

Figure 3-13: Test Case Corner Pressure Time History

[

]

Figure 3-14: Test Case Pressure Time History at the Wall

[ ]

3.3.2.4 Sensitivity Study

[ ]

[

]

3.3.2.5 Spatial Discretization

[

]

[

]

3.4 *Structural Evaluation of Typical Target Essential SSC*

[

]

3.4.1 Dynamic Finite Element Analysis

The response of essential SSC that may only be considered as multi-degree of freedom structures is typically determined through finite element analysis, using beam models, plate and shell models, or a combination of the two. Figure 3-16 illustrates a typical plate and shell finite element model of a steam generator from the U.S. EPR. This model is used to perform stress analyses and to determine the dynamic response to a jet impingement load on the steam drum region.

The general analytical methodology for determining the dynamic response of a structure to jet impingement or blast loads is as follows:

- Develop a finite element model of the structure using codes such as BWSPAN (beam element models) or ANSYS (plate and shell element models).
- Perform modal analyses to identify the structural frequencies and mode shapes of the target structure.
- Develop forcing functions representing jet impingement or blast loads. Jet impingement forcing functions are expressed as sinusoidal time histories with the magnitudes representative of the jet force amplitude (as derived in Section 3.2.5.2). The frequencies of oscillation are developed to match the structural frequencies of interest. Blast forcing functions are often represented as triangular pulse loads with calculated duration. However, in cases where reflections exist, it is often necessary to use a time history approach with pressures directly from the CFD analysis.
- Perform transient dynamic analyses using the Direct Integration or Modal Superposition method of solution.
- Perform a frequency sweep analysis to identify the modes with the largest dynamic response to the applied forcing function. The displacement, and subsequently the stress, response will generally peak within the first few structural modes and then reduce significantly for higher modes. Determine the appropriate cutoff frequency using the criteria provided by Section 3.4.1.4.

3.4.1.1 Modeling

There are two types of structural response that must be considered for any target SSC, local and global.

- Local response can be significant in plate and shell structures (e.g., pressure vessels) and involves out of plane bending modes. Figure 3-15 illustrates typical mode shapes for an edge supported rectangular plate. In plate and shell element models, the mass is distributed evenly; therefore, mass point spacing is not considered critical. Sensitivity studies are typically performed to determine proper meshing schemes for accurate calculation of frequencies in excess of the jet resonant frequency and the frequency of maximum response or periods in excess of the blast pulse duration. Note that the frequency of maximum response is typically one of the first few shell modes because the response of higher order modes gives smaller displacements.
- Global response can be significant in any structure and is often modeled with beam elements. To properly define the modes of vibration for a beam, enough node points and mass points must be included in the model. Mass point spacing for beam element dynamic models is critical in determining frequencies of higher order modes. The maximum mass point spacing for a lumped mass model is determined as discussed in Reference 9.
- Stress results are critical in modeling, particularly in determining local response. As is often done with finite element analyses for other loading mechanisms, sensitivity studies are performed to ensure that the maximum stress is properly accounted for in the analysis. This may be done by using increasingly fine meshes until convergence of results is obtained. U.S. EPR FSAR Tier 2, Section 3.9.3, describes the design and analyses related to the structural integrity of ASME Code Class 1, 2, and 3 Components, Component Supports and other essential SSC. The loading combinations and acceptance criteria for these are provided in U.S. EPR FSAR Tier 2, Tables 3.9.3-1 through 3.9.3-4.

3.4.1.2 Damping

Damping is selected based on the type of analysis and response being calculated. When finite element analyses are performed to determine the high frequency (i.e., > 33 Hz) local and global response in plate and shell structures due to jet impingement, 1% damping is used because the strain in high frequency modes is lower than would be expected from lower frequency modes.

When it is required that Rayleigh damping be used, the alpha and beta values are selected so that total damping at the key frequencies of the SSC is equivalent to the 1% damping value selected. The equation to determine mass and stiffness proportional damping using the Rayleigh method is as follows:

$$\zeta = \frac{\alpha}{2\omega} + \frac{\beta\omega}{2}$$

Where:

ζ = Critical Damping Ratio

α = Mass Proportional Damping Coefficient

β = Stiffness Proportional Damping Coefficient

ω = Target SSC Natural Frequency in radians/sec

The values alpha (α) and beta (β) are unknowns that are solved using the desired critical damping ratio and known natural frequencies.

In cases where modal damping can be used, the 1% damping value may be input without additional calculations.

In accordance with RG 1.61, analyses use viscous damping. This is acceptable from a structural analysis perspective because the structures are assumed to be in phase with the loading mechanism, thereby alleviating the need for consideration of structural loss factors and phase angles.

3.4.1.3 Loading Method

The method used for applying jet impingement and blast loading depends on the type of analysis being performed, local or global, as follows:

3.4.1.3.1 Jet Impingement Loading Method

[ ]

3.4.1.3.2 Blast Loading Method

[ ]

- [

]

- [

]

3.4.1.4 Cutoff Frequency Criteria

3.4.1.4.1 Jet Impingement Loading

The criteria used to determine the minimum cutoff frequencies for target SSC under jet impingement loading are developed based on analysis and theory. The criteria are slightly different for plate and shell structures, such as pressure vessels, and beam-type structures, as follows:

- For plate and shell structures, that is structures with local response modes, frequencies up to the greater of twice the maximum response frequency and 500 Hz should be considered, and should provide a reduction in modal response of at least 75% from that of the maximum response frequency. If a reduction in response of at least 75% is not seen, additional frequencies should be considered to demonstrate that the dominant mode of vibration has been determined.

- For beam-type structures, that is structures with only global response modes, enough frequencies must be considered to achieve a cumulative effective mass of 95% of the target SSC total mass. The effective mass for a given frequency is calculated as the square of the participation factor (Γ_n). Any remaining mass is accounted for using the "missing mass" approach, as discussed in Reference 9. This approach provides a residual mode shape but does not correspond to a frequency. When a time history is applied to a beam-type structure and the missing mass approach is used, the residual mode shape is loaded in addition to the lower frequency modes of the model.

Dynamic Analysis Theory

The general equation to determine dynamic modal response of a target SSC, from Reference 24, is:

$$U_{no} = (P_o)(R_{Dn})(\Gamma_n)(\Phi_n)/\omega_n^2$$

Where:

P_o = Force Amplitude

R_{Dn} = Dynamic Displacement Response Factor at nth mode of vibration

Γ_n = Modal Participation Factor

Φ_n = Mode Shape Vector for n^{th} mode

ω_n = Target SSC Natural Frequency in radians/sec

As shown in the equation, the square of the frequency (ω_n) is in the denominator. The modal response is, therefore, inversely proportional to the square of the frequency. For modes with equivalent mode shape displacements and participation factors at two different frequencies, the mode with the greater frequency gives reduced displacement response and, consequently, reduced stress intensities. In a case where one of the two modes has a frequency twice that of the other mode, the resulting response would be approximately 75% lower for the higher frequency mode.

Analytical Results

The example results provided in Section 3.4.1.5 demonstrate that, for a typical target SSC, such as a pressure vessel, the graph of response exhibits several peaks up to approximately 500 Hz. At this point, the graph of response becomes relatively smooth and trends in the downward direction.

3.4.1.4.2 Blast Loading

The criteria used to determine the minimum cutoff frequencies for target SSC under blast loading are developed based on analysis and theory. The criteria are the same for plate and shell structures and beam-type structures, as follows:

Blast loading is a noncyclic impulse load. Therefore, the minimum cutoff frequency must only be great enough to ensure that the structure is capable of responding to the rapid pulse loading. In order for the half-period of the structure to be short enough to respond to the time duration of the initial pulse (t_d – Figure 3-9), the period of the structure must be no greater than the time duration of the blast initial pulse, giving a minimum cutoff frequency of $1/t_d$.

3.4.1.5 Example Results

An example of a typical dynamic finite element analysis result is provided in Figure 3-17 for the model illustrated in Figure 3-16. In this analysis, a sinusoidal force with amplitude of approximately 94,000 lbs is applied to the upper shell portion of the component at each of the natural frequencies of the model up to 2000 Hz. As shown in Figure 3-17, the stress intensity peaks at relatively low frequency (<100 Hz) but continues to show significant stresses, although approximately 50% lower than the maximum stress intensity, at frequencies up to approximately 500 Hz.

This is a specific example and is not intended to provide a bounding analysis for other components. However, this example does provide insight into the variation of stress response with frequency. As shown in Figure 3-17, the stress intensity decreases by approximately 75% at 1000 Hz. At this frequency, based on the smooth downward trend of the stress results, the frequency with the maximum stress response has been considered.

Using the specific criteria discussed in Section 3.4.1 along with the example results provided in Figure 3-17, a determination of required cutoff frequency can be made. The provided criteria are as follows:

- For plate and shell structures, frequencies up to the greater of twice the maximum response frequency or 500 Hz should be considered.
- A reduction in modal response of at least 75% from that of the maximum response frequency should be seen.
- If a reduction in response of at least 75% is not seen, additional frequencies should be considered in order to demonstrate that the dominant mode of vibration has been determined.
- Based on these criteria, the required natural frequency, based on a reduction in response of 75%, is 1000 Hz.

Figure 3-15: Rectangular Plate Mode Shapes

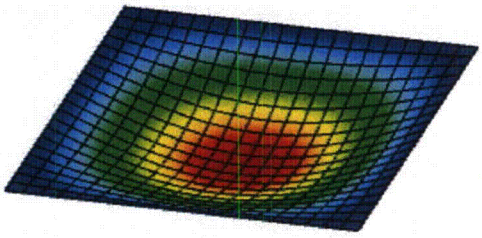

Mode 1:

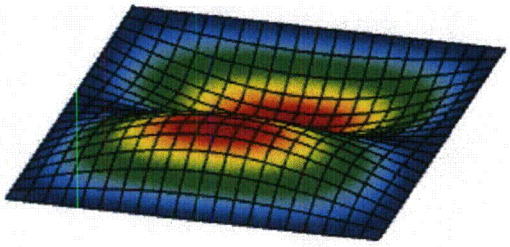

Mode 2:

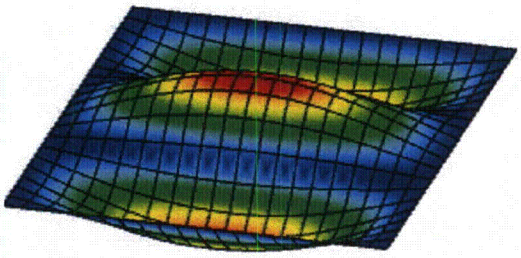

Mode 3:

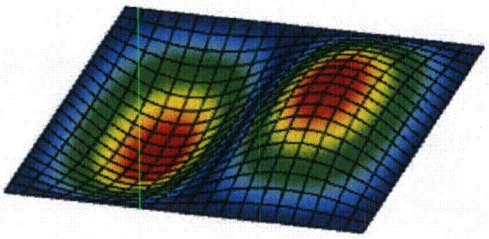

Mode 4:

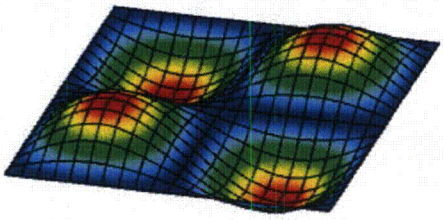

Mode 5:

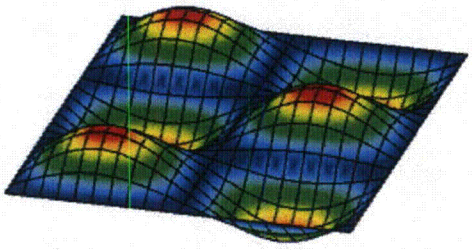

Mode 6:

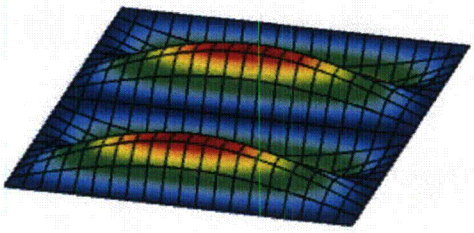

Mode 7:

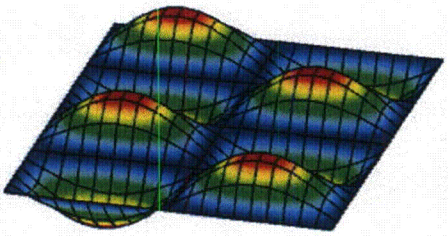

Mode 8:

Figure 3-16: Typical Plate and Shell Finite Element Model

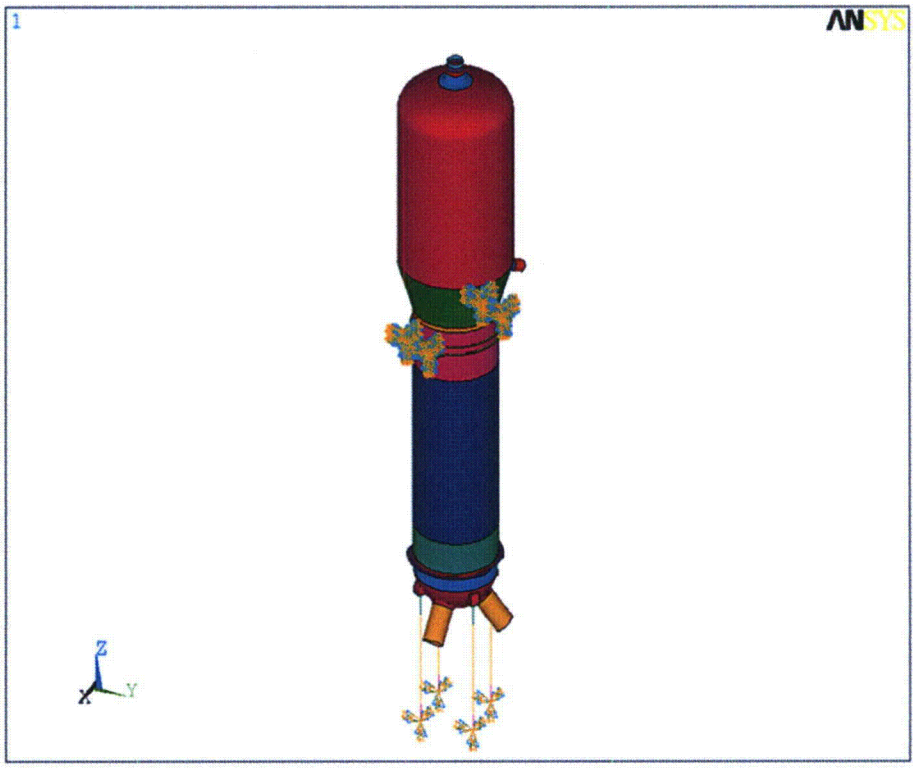

Figure 3-17: Shell Stress Intensity vs. Load Frequency

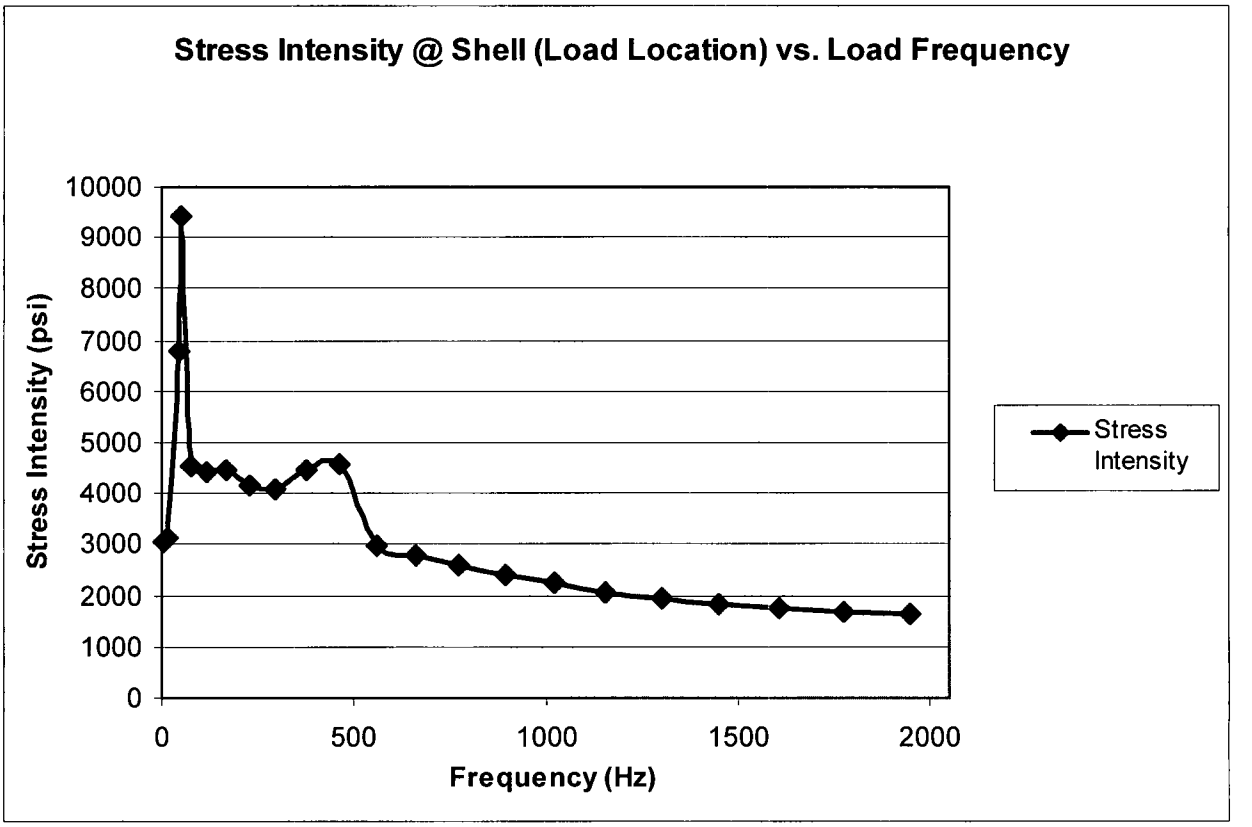

3.4.2 Static Analysis using Dynamic Load Factors

Hand calculations or finite element analyses using dynamic load factors may be used to accurately predict the response of essential SSC that may be idealized as single degree of freedom oscillators to a pulse or sinusoidal forcing function. Pulse forcing functions associated with pipe rupture would be caused by the initial stage of jet impingement or by blast waves. The procedure for performing structural evaluations of simple structures through hand calculations or finite element analysis is as follows:

- Determine structure's dominant natural frequency.
- Define blast and jet impingement pulse dynamic loading.
- Define jet impingement resonant dynamic loading.
- Determine dynamic load factor for each type of loading, using Reference 17, or similar.

- Determine maximum response and member loads/stresses for comparison to applicable code allowables.

This approach requires the analyst to evaluate its applicability to the structure and loading in question. This method is generally applicable to structures and loadings in which:

- The resistance function of the structure (the spring rate) is linear and may be determined through hand calculations or simple computer models.
- The mode shape of the dominant mode may be determined based on the characteristics of the structure and its support system (such as a cantilevered beam or simply supported beam).
- The natural frequency for the dominant mode may be determined based on the mass and stiffness of the structure and the definition of the applied loading.
- The applied loading direction and location corresponds to the shape and direction of the dominant mode.
- The loading may be defined as a triangular or rectangular pulse or as a sinusoidal function.
- The structure does not exhibit significant localized deflections due to the applied loading.

3.4.3 Analysis Methodology Steps

Figure 3-18 provides a flow chart illustrating the basic steps taken to determine jet impingement and blast loads and their application to target SSC.

Figure 3-18: Loading Analysis Methodology Flow Chart

3.5 *Applicable Codes and Standards*

Essential target SSCs are evaluated in accordance with applicable codes and standards for the item in question. The following codes and standards provide the design requirements for typical SSC in the U.S. EPR:

- ASME Section III Boiler and Pressure Vessel Code, 2004 Edition (Reference 25).
- AISC N-690, 1994 Edition, including Supplement 2 (2004) (Reference 18).
- ACI 349, 2001 Edition (Reference 19).

Deformation in steel and concrete non-pressure retaining SSC under impulsive loads is controlled by limiting the ductility ratio, μ_d, defined as the ratio of maximum acceptable displacement, X_m, (or maximum strain, ε_m) to the displacement at the effective yield point, X_y, (or yield strain, ε_y) of the structural element. In addition to the specified deformation limits, the maximum deformation shall not result in the loss of intended function of the structural element nor impair the safety-related function of other systems and components. In the evaluation of the overall response of reinforced concrete and steel structures subject to impulsive loads, it is acceptable to assume non-linear (elasto-plastic) response of the structural elements.

The following sections briefly describe the basic design requirements for essential SSCs in the U.S. EPR, including areas where nonlinear elastic-plastic analysis may be used.

3.5.1 Pressure Vessel Code Requirements

Level D events (e.g., pipe rupture) are evaluated in accordance with Appendix F of the ASME Code, Section III (Reference 25). The basic requirement found in Appendix F, Paragraph F-1331.1, when using elastic analysis, is that primary membrane stresses shall not exceed 70% of the material tensile strength (Reference 25, F-1331). This implies a minimum margin in excess of 40% (1/0.7 – 1 = 0.43).

3.5.2 Steel Structure Code Requirements

Reference 18 provides design requirements for steel structures under abnormal loading, such as during a pipe rupture event. When performing linear elastic analysis, most tension allowable stresses are increased by 60% over the normal allowable stresses except that these stresses shall not exceed 70% of the material tensile strength (Reference 18, Table Q1.5.7.1). This implies a minimum margin in excess of 40%, which is the same as that of ASME piping and components required to maintain pressure boundary, as discussed in Section 3.5.1. When performing nonlinear elastic-plastic analysis, the allowable ductility ratio for beams in flexure with open and closed sections must be maintained below the maximum allowable values of 12.5 and 20, respectively, per Reference 18, Table Q1.5.8.1.

3.5.3 Concrete Structure Code Requirements

Reference 19 provides design requirements for concrete structures under abnormal loading (e.g., during a pipe rupture event). The strength design method is used for the structural analysis of concrete, which required the application of load factors (Section 9.2 of Reference 19) and design strength reduction factors (Section 9.3 of Reference 19). Appendix C of Reference 19 also provides special provisions for impulsive loading on concrete, which allows the use of ductility ratios. The provisions provide a minimum safety margin of 20% to the ultimate strength of concrete for impulsive loading per Section C.3.2 of Reference 19. When performing nonlinear elastic-plastic analysis, the allowable ductility ratio for a beam, wall or slab in flexure is dependent on the reinforcement ratio, but must be maintained below the maximum allowable value of 10 (Reference 19, Section C.3.2).

4.0 REFERENCES

1. NUREG-0800, Standard Review Plan 3.6.2, Rev. 2, "Determination of Rupture Locations and Dynamic Effects Associated with the Postulated Rupture of Piping, " March 2007.
2. ANSI/ANS Standard 58.2-1988, "Design Basis for Protection of Light Water Nuclear Power Plants Against the Effects of Postulated Pipe Rupture," American Nuclear Society 1988.
3. Wallis, G., "The ANSI/ANS Standard 58.2-1988: Two Phase Jet Model," September 15, 2004.
4. Ransom, V., "Comments on GSI-191 Models for Debris Generation," September 14, 2004.
5. NUREG-0800, Branch Technical Position 3-4, Rev. 2, "Postulated Rupture Locations in Fluid System Piping Inside and Outside Containment," March 2007.
6. NUREG/CR-2913, "Two-Phase Jet Loads," Nuclear Regulatory Commission, January 1983.
7. Shapiro, Ascher, "The Dynamics and Thermodynamics of Compressible Fluid Flow," 1953, John Wiley and Sons.
8. NUREG-0800, Branch Technical Position 3-3, Rev. 3, "Protection Against Postulated Piping Failures in Fluid System Piping Outside Containment," March 2007.
9. ANP-10264NP-A, Revision 0, "U.S. EPR Piping Analysis and Pipe Support Design Topical Report," AREVA NP Inc., November 2008.
10. NEA Report NEA/CSNI/R (95)11, "Knowledge Base for Emergency Core Cooling System Recirculation Reliability", February 1996.

11. Nosseir, N. S. and Ho, C-M., "On the Feedback Phenomenon of an Impinging Jet," September 1979.

12. Nosseir, N. S. and Ho, C-M., "Dynamics of an Impinging Jet. Part 1. The Feedback Phenomenon," Journal of Fluid Mechanics, Vol. 105, pp. 119 – 142, 1981.

13. Tam, C. K. W. and Ahuja, K. K., "Theoretical Model of Discrete Tone Generation by Impinging Jets," Journal of Fluid Mechanics, Vol. 214, pp. 67 – 87, 1990.

14. Henderson, B., "The Connection between Sound Production and Jet Structure of the Supersonic Impinging Jet," Journal of the Acoustical Society of America, Vol. 111, pp. 735 – 747, February 2002.

15. Kim, S. I. and Park, S. O., "Oscillatory Behavior of Supersonic Impinging Jet Flows," Copyright Springer-Verlag, 2005.

16. Isozaki, T. and Miyazono, S., "Experimental Study of Jet Discharging Test Results Under BWR and PWR Loss of Coolant Accident Conditions," Nuclear Engineering and Design, Vol. 96, pp. 1 – 9, 1986.

17. Biggs, J. M., "Introduction to Structural Dynamics," 1964, McGraw-Hill.

18. AISC N690-1994(R2004), "Specification for the Design, Fabrication and Erection of Steel Safety-Related Structures for Nuclear Facilities," including Supplement 2, American National Standards Institute, 2004.

19. ACI 349-01, "Code Requirements for Nuclear Safety-Related Concrete Structures" American Concrete Institute, 2001.

20. Army TM 5-1300/Navy NAVFAC P-397/Air Force AFR 88-22, "Joint Departments of the Army, the Navy, and the Air Force, Structures to Resist the Effects of Accidental Explosions," November 1990.

21. Kinney, G. and Graham, K., "Explosive Shocks in Air," Springer-Verlag, New York, 1985.

22. Letter, Rowley, J. (NRC) to Nowinowski, A. (Westinghouse), Subject: Nuclear Regulatory Commission Conclusions Regarding Pressurized Water Reactor Owners Group Response to Request for Additional Information, dated January 25, 2010, Regarding Licensee Debris Generation Assumptions for GSI-191, Accession Number: ML100570364.

23. NASA Contractor Report NASA CR-2843, "Measurement of Blast Waves from Bursting Pressurized Frangible Spheres", May,1977.

24. Chopra, A. K., "Dynamics of Structures, Theory, and Applications to Earthquake Engineering," 1995, Prentice-Hall.

25. ASME Boiler and Pressure Vessel Code, Section III, "Rules for Construction of Nuclear Facility Components," The American Society of Mechanical Engineers, 2004.

26. Becht, C. and Moody, F. J., "Analysis Techniques for Modeling the Pressure Wave Effects of Guillotine Ruptures of Steam Lines", Proceedings of the ASME 2011 Pressure Vessels & Piping Division Conference, July 17-21, Baltimore, Maryland, USA, 2011.

27. ANSYS Documentation, Version 14.5, ANSYS, Inc., Southpointe, 275 Technology Drive, Canonsburg, PA 15317.

28. Isaev, S. A. and Lysenko, D. A., "Testing of Numerical Methods, Convective Schemes, Algorithms for Approximation of Flows, and Grid Structures by the Example of a Supersonic Flow in a Step-Shaped Channel with the Use of the CFX and FLUENT Packages," Journal of Engineering Physics and Thermophysics, Vol. 82, No. 2, 2009.

29. Thallam Thattai, A., "A Validation Study for Turbulent Premixed Flame Propagation in Closed Vessels," Master's Thesis, Delft University of Technology, 2010.

30. Absil, L. H. J., van den Berg A. C., and Weerheijm J. C. MABS 13, 13th Int. Symposium on the Military Application of Blast Simulation, The Hague, The Netherlands, 1993.

31. Absil, L. H. J., Kodde H. H., et al., Details of Blast Interaction with Structure," Proceedings of the Twenty-sixth Explosives Safety Seminar, Miami, FL, August 16-18, 1994.

32. Van Wingerden, K., Hansen, O. R., and Foisselon, P., "Predicting Blast Overpressures Caused by Vapor Cloud Explosions in the Vicinity of Control Rooms," Process Safety Progress, Vol. 18, No. 1, 1999.

33. Woodward, P. and Colella, P., "The Numerical Simulation of Two-Dimensional Fluid Flow with Strong Shocks," Journal of Computational Physics, 54, 115-173, 1984.

34. Trélat, S., Sochet, I., et al., "Blast Wave on a Parallelepipedic Obstacle," 20th International Colloquium on the Dynamics of Explosions and Reactive Systems (ICDERS), July 31 to August 5, 2005.

35. Chandra, N. et al., "Evolution of Blast Wave Profiles in Simulated Air Blasts - Experiment and Computational Modeling," Shock Waves, 22, 2012.

APPENDIX A
CFD CODE VALIDATION

A.1 Objectives and Scope

The purpose of this appendix is to describe and validate the methods used to calculate the blast effects which generate pressure loads on internal structures, using CFD analysis. The methodology considers the numerical approaches used by CFD. The CFD code used for this purpose is [ ]

Later versions of this software are acceptable for use, provided the results are validated against the results of the version considered in this report.

Two experimental tests were selected from the open literature to serve as validation cases for the developed methodology. The comparison between CFD results and measured data demonstrates the capability of the CFD code to calculate physical phenomena related to blast effects

A.2 Problem Description

The postulated rupture of a high energy line in a containment room involves physical phenomena related to blast effects. A high energy line is a pipe with high temperature and pressure fluid exceeding either 200°F or 275 psig during normal operating conditions.

The blast effect is illustrated in Figure A.2-1. The large amount of energy in the fluid (steam) is released suddenly into the surrounding air. This rapid gas expansion forces out the volume it occupies and a layer of compressed air is created in front of this gas volume. A pressure front associated with the high pressure gas propagates radially into the surrounding air as a strong shock wave. This shock front is the blast wave, which is characterized by an almost instantaneous increase from the ambient pressure to a peak incident pressure.

Figure A.2-1: Simplified Blast Wave Formation from a High-Energy Line Rupture

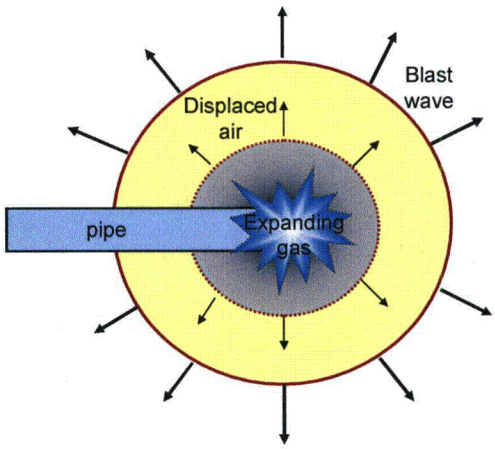

Figure A.2-2 shows a typical blast pressure time history with the following main parameters:

t_a	=	Arrival time following the rupture
t_d	=	Duration of the positive phase
P_y , p^0 or P_{peak}	=	Peak overpressure
P_x or P_o	=	Ambient pressure

Figure A.2-2: Typical Blast Pressure-Time History

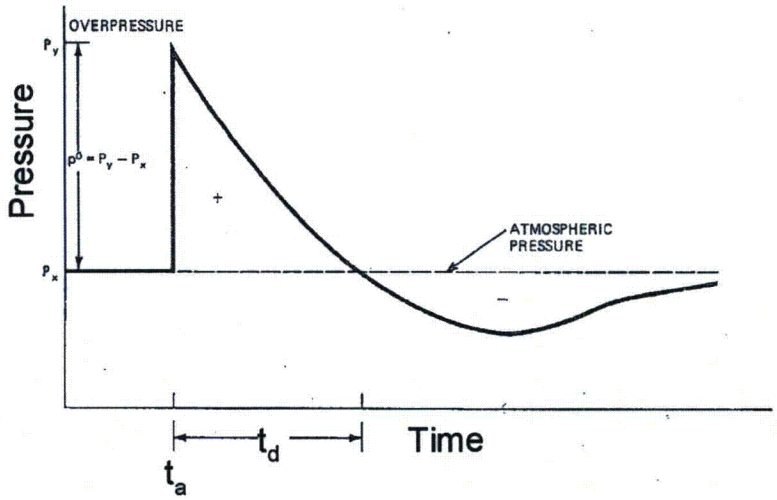

As the blast wave propagates three-dimensionally in the room, the shock front may strike obstacles (e.g., walls or other internal structures within the containment). The interaction of the incident blast wave with obstacles causes reflections and the peak incident pressure is amplified by a reflection factor. The reflected pressure is higher than the peak incident pressure. The magnitude of the blast loads on the obstacle depends on following factors:

- Amount of energy released by the pipe rupture in form of a blast wave.
- Distance between rupture and obstacle.
- Reflection factor (amplification) of the pressure by the interaction with the ground or obstacle itself.

The generated blast pressure from the pipe rupture is often magnified by nearby structures, especially the walls normal to the blast wave. The distribution of the loads on the surfaces is non-uniform with the maximum load typically occurring on the surface closest to the blast origin location.

The developed methodology using CFD approaches consists of predicting the formation of the blast wave from a given energy source, the propagation of the shock front, and the prediction of the pressure loads derived by interactions with obstacles and multiple reflections. This methodology is validated against suitable experimental data obtained in open literature.

A.3 Methodology

[

]

[

]

[

]

A.3.1 CFD Approach

[

]

A.3.1.1 Physical Models

[

]

A.3.1.2 Solver

[

]

[

]

A.3.1.3 Numerical Solution Scheme

[

]

[

]

A.3.1.4 ANSYS FLUENT Reference Settings

[

]

Table A.3-1: Summary of Reference Settings for Blast Wave Application

[

]

A.4 Code Validation

[

]

A.4.1 Blast Interaction with Multiple Obstacles (2D and 3D Calculations)

[

]

Figure A.4-1: Experimental Test Configuration (Reference 29)

[

]

Figure A.4-2: Dimensions of the Shock Tube Test and Positions of the Pressure Transducers

[

]

[

Initial Conditions and Boundary Conditions

[

]

[

]

CFD Model Initial Conditions and Boundary Conditions

[

]

Figure A.4-3: CFD 3D-Model and Boundary Conditions

[

]

Figure A.4-4: Pressure-Time Profile Used as Input for Simulations (Red line)

Figure A.4-5: Peak Pressure of a Blast Wave Propagation as Function of Distance (Reference 34)

[

]

A.4.1.1 Settings and Solver Details

[

]

A.4.2 Results

[

]

First Configuration

[

]

[

]

Table A.4-1: Reference 2D Mesh for the First Configuration

[

]

[

]

Figure A.4-6: Comparison of Experimental and Calculated Interferograms

[

]

Second Configuration

[

]

Table A.4-2: Used 2D Meshes for the Second Configuration

[ ]

[

]

Figure A.4-7: Comparison of 2D and 3D Models Using the Coarse Mesh

[

[

]

Figure A.4-8: Comparison between Turbulent and Inviscid Flow

[

]

[

]

Figure A.4-9: Comparison between "Ideal Gas" and "Real Gas"

[

]

A.4.2.1 Mesh Sensitivity

[

]

Figure A.4-10: Comparison between Models Using Different Meshes

[ ]

[

]

Figure A.4-11: Comparison between Models Using Different Mesh Sizes

[ ]

A.4.2.2 Time Step Sensitivity

[

]

Figure A.4-12: Comparison between Models using Different Courant Numbers

[ ]

A.4.2.3 Model Improvements

[

]

Figure A.4-13: Comparison between Models Using Different Parameters D_{outlet}

[ ]

[

]

Figure A.4-14: Pressure-Time History in Position 1 from Experiments and from Simulations using Two Different Parameters D_{inlet}

[

]

[

]

Figure A.4-15: Deviation in the Pressure-Time History Caused by the Reflected Wave from the Inlet Boundary

[

]

Table A.4-3: Overpressure Peak Obtained as Function of the Input Data for Incoming Blast Wave

[ ]

A.4.2.4 Full Validation

Figure A.4-16: Comparison between Measured and Calculated Pressure-Time History

Figure A.4-17: Comparison between Measured and Calculated Pressure-Time History at Position 3

Figure A.4-18: Comparison between Measured and Calculated Pressure-Time History at Position 4

A.4.3 3D Blast Wave on Parallelepipedic Obstacle

[

]

Figure A.4-19: Experimental Configuration of the Detonation of Propane in Front of a Parallelepipedic Structure

[

]

A.4.3.1 Initial and Boundary Conditions

[

]

A.4.3.2 CFD Model

[

]

Figure A.4-20: CFD Model (Left) and Mesh (Right) of the Experiment

[

]

A.4.3.3 Settings and Solver Details

[

]

A.4.3.4 Results

Figure A.4-21: Measured and Calculated Reflected Pressure-Time Histories

A.5 Conclusions

[

]

APPENDIX B
CFD SAMPLE PROBLEM

B.1 Objectives and Scope

[

]

B.2 Problem Description

[

]

B.2.1 Geometry

[

]

Figure B.2-1: Sample Problem Geometry – Plan View

Figure B.2-2: Sample Problem Geometry – Elevation View

Figure B.2-3: CFD Model Internal Structures and Initial Conditions

B.2.2 Meshing

[

]

[

]

Table B.2-1: CFD Model Mesh Development Data

[

]

Figure B.2-4: Elevation View of N4 and N5 Meshes at Plane through Pipe Rupture Point

Figure B.2-5: Plan View of N4 and N5 Meshes at Plane through Pipe Rupture Point

B.2.3 Boundary Conditions

[

]

B.2.4 Modeling Details

[

]

Table B.2-2: Validated CFD Analysis Base Settings

[

]

B.3 Monitoring Pressure Loads

Figure B.3-1: Monitor Points in the Jet Stream Path

Figure B.3-2: Wall Monitor Points

[ ]

B.4 Pressure Loads

[

]

Figure B.4-1: Blast Wave Characteristics at Time = 0.000392 sec

Figure B.4-2: Elevation View of Pressure Field vs. Time

Figure B.4-3: Plan View of Pressure Field vs. Time

Figure B.4-4: Pressure Time History Curve for Monitor Points

Figure B.4-5: Blast Pressures vs. Time

Figure B.4-6: Steam Impingement on Walls at Time = 0.00866 Seconds

Figure B.4-7: Steam Plume and Distribution at Time = 0.00403 Seconds

Figure B.4-8: Target Wall Pressure Time Histories

Figure B.4-9: Target Wall Corner Region Pressure Time Histories

Figure B.4-10: Left Wall Pressure Time Histories

B.5 Mesh Sensitivity

[

]

Figure B.5-1: Mesh Specific Target Wall Pressure Time Histories (Points 1 – 8)

Figure B.5-2: Mesh Specific Target Wall Pressure Time Histories (Points 9 – 16)

Figure B.5-3: Mesh-Specific Target Wall Pressure Time Histories (Points 17 - 18)

Figure B.5-4: Meshes N5 and N6 Pressure Peak Deviations

Figure B.5-5: Meshes N4 and N6 Pressure Peak Deviations

Figure B.5-6: Meshes N1 and N6 Pressure Peak Deviations

B.6 Conclusion